Chapter 11
The Use of Fiber Bragg Grating Sensors for Strain Modal Analysis

Fábio Luis Marques dos Santos, Bart Peeters, Ludo Gielen, Wim Desmet, and Luiz Carlos Sandoval Góes

Abstract This paper discusses the use optical fiber Bragg grating (FBG) strain sensors for structural dynamics measurements and modal analysis. For some industrial applications, the use of strain sensors (combined or not with accelerometers) can bring benefits such as reduced size and weight. In many of these applications, FBG sensors lead the class of new sensor technologies that make dynamic strain measurements more attractive, with additional qualities such as the reduction of cabling, immunity to electromagnetic interference and higher sensor robustness. On the other hand, the main difficulty in the use of this technology is their integration and synchronization with other types of sensors, since their acquisition usually requires a separate specialized measurement unit. This is an important requirement in modal analysis, where synchronization between input and output measurements is a key issue that can directly affect the quality of the data. In this paper, FBG sensors are used in an experimental modal analysis, where their analogue signal is digitalized on the same way as the electrical sensors, guaranteeing synchronization.

Keywords Strain modal analysis • Dynamic strain • Strain field • Fiber bragg grating • Strain mode shape

11.1 Introduction

Strain gauges have been commonly used for static load testing, durability analysis and lifetime prediction in the mechanical industry [1–3]. Moreover, there are applications in which dynamic strain measurements are more usual, such as in load identification in Transfer Path Analysis, or sometimes the sensor size makes it for a more suitable choice, which is the case for gas turbine blade testing or helicopter and wind turbine blade measurements. Another application that can use dynamic strain measurements is strain modal analysis. Usually modal testing has been associated with the use of displacement responses (or their derivatives with respect to time), but the use of strain sensors for modal testing has been already discussed [4–7]. Recently there has been growing interest from both industry [8] and academia [9] on the topic—assessing and evaluating structural integrity on design prototype stages and also monitoring in real-time (with structural health monitoring systems (SHM)) has led to an increase in the number of dynamic strain applications, to the development of improved identification and measurement techniques, as well as to improved sensor technology.

F.L.M. dos Santos (✉)
Siemens Industry Software, Interleuvenlaan 68, 3001 Leuven, Belgium

Katholieke Universiteit Leuven (KUL), Division PMA, Celestijnenlaan 300B, 3001 Heverlee, Belgium
e-mail: fabio.m.santos@siemens.com

Institute Tecnológico de Aeronáutica (ITA), Praça Marechal Eduardo Gomes,
50-Vila das Acácias CEP 12.228-900 São José dos Campos SP, Brazil

B. Peeters • L. Gielen
Siemens Industry Software, Interleuvenlaan 68, 3001 Leuven, Belgium
e-mail: bart.peeters@siemens.com; ludo.gielen@siemens.com

W. Desmet
Katholieke Universiteit Leuven (KUL), Division PMA, Celestijnenlaan 300B, 3001 Heverlee, Belgium
e-mail: wim.desmet@kuleuven.be

L.C.S. Góes
Institute Tecnológico de Aeronáutica (ITA), Praça Marechal Eduardo Gomes,
50-Vila das Acácias CEP 12.228-900 São José dos Campos SP, Brazil
e-mail: goes@ita.br

M. Mains (ed.), *Topics in Modal Analysis, Volume 10*, Conference Proceedings of the Society
for Experimental Mechanics Series, DOI 10.1007/978-3-319-15251-6_11

A recent and important contribution on the field of dynamic strain measurements are the fiber optic sensors, of which the most popular types are the Fiber Bragg Grating (FBG) sensors [10, 11]. Some of their advantages are robustness to magnetic interference, small sensor dimensions and weight, reduced cabling, possibility to embed on composites plus the possibility of embedding these sensors in composite structures, makes for an attractive solution for use in SHM systems. The availability of such an array of sensors, ready to be used and adequate for modal testing, is another incentive to carrying out a strain modal analysis, saving up on time and instrumentation.

Another application of dynamic strain measurements is related to the strain displacement relations [12]. In many systems, strain gauges are used as the standard vibration sensor, especially when size or sensor location is an issue. Such is the case in aerospace applications, like gas turbines, wind turbines and helicopters [13], where size and weight are very restricted, and any sensor place on a blade should affect its aerodynamic properties as little as possible. One particular use of the strain measurements and strain to displacement relations is the strain pattern analysis (SPA), where strain measurements are used to predict blade displacements.

11.2 Strain Modal Analysis Theory

To obtain the strain modal formulation, one can start with the fundamental theory of modal analysis. Modal theory states that the displacement on a given coordinate can be approximated by the summation of a n number of modes:

$$u(t) = \sum_{i=1}^{n} \phi_i q_i(t) \tag{11.1}$$

where u is the displacement response in x direction, ϕ_i is the ith (displacement) vibration mode, and q_i is the generalized modal coordinate and t is time. For small displacements, given the theory of elasticity, the strain/displacement relation is:

$$\varepsilon_x = \frac{\partial}{\partial x} u \tag{11.2}$$

And similarly, the same relationship exists between the strain vibration modes and the displacement modes:

$$\psi_i = \frac{\partial}{\partial x} \phi_i \tag{11.3}$$

This way, by the relations on Eqs. (11.2) and (11.3), the expression on (11.1) can be rewritten as:

$$\varepsilon(t) = \sum_{i=1}^{n} \psi_i q_i(t) \tag{11.4}$$

Moreover, the relationship between the generalized modal coordinate q and an input force F is:

$$q_i = \Lambda_i^{-1} \phi_i F, \text{with} \Lambda_i = (-\omega^2 m_i + j\omega c_i + k_i) \tag{11.5}$$

where m_i, c_i and k_i are the ith modal mass, modal damping and modal stiffness, and ω is the excitation frequency.

Substituting (11.5) into (11.4), the relation between a force input and a strain output, in terms of displacement and strain modes is represented as:

$$\varepsilon_i = \sum_{i=1}^{n} \psi_i \Lambda_i^{-1} \phi_i F \tag{11.6}$$

And finally, the strain frequency response function (SFRF) can be obtained, in matrix form:

$$[H^{\varepsilon}] = \sum_{i=1}^{n} \Lambda_i^{-1} \{\psi_i\} \{\phi_i\} = [\psi] [\Lambda]^{-1} [\phi]^T \tag{11.7}$$

The expansion of (11.7) is:

$$\begin{bmatrix} H^{\varepsilon}_{11} & H^{\varepsilon}_{12} & \cdots & H^{\varepsilon}_{1N_i} \\ H^{\varepsilon}_{21} & H^{\varepsilon}_{22} & \cdots & H^{\varepsilon}_{2N_i} \\ \vdots & \vdots & \vdots & \vdots \\ H^{\varepsilon}_{N_o1} & H^{\varepsilon}_{N_o2} & \cdots & H^{\varepsilon}_{N_oN_i} \end{bmatrix} = \sum_{i=1}^{n} \Lambda_i^{-1} \cdot \begin{bmatrix} \psi_{1i}\phi_{1i} & \psi_{1i}\phi_{2i} & \cdots & \psi_{1i}\phi_{N_i i} \\ \psi_{2i}\phi_{1i} & \psi_{2i}\phi_{2i} & \cdots & \psi_{2i}\phi_{N_i i} \\ \vdots & \vdots & \vdots & \vdots \\ \psi_{N_o i}\phi_{1i} & \psi_{N_o i}\phi_{2i} & \cdots & \psi_{N_o i}\phi_{N_i i} \end{bmatrix} \tag{11.8}$$

where N_o represents the number of strain gauge measurement stations (or the number of output measurements) and N_i represents the number of excitation points (or the number of inputs).

The columns of the matrix correspond to the strain responses due to the excitation points along the rows of the matrix. Some important characteristics can be inferred from Eq. (11.8). First of all, differently from displacement FRFs, the SFRF matrix is not symmetric, that is, for instance, $H^{\varepsilon}_{12} \neq H^{\varepsilon}_{21}$. This means that reciprocity is not guaranteed for strain modal analysis—exciting point a and measuring point b will not yield the same FRF as if exciting point b and measuring point a. Moreover, any column of the SFRF matrix contains all the information regarding the strain modes (ψ), while any row of the SFRF matrix contains information about the displacement modes (ϕ). This particular property leads to practical applications—to obtain the strain mode shapes, one must use a fixed excitation point and measure the strain responses. On the other hand, by using a strain gauge as a fixed reference sensor and moving the excitation point (as with impact testing), the displacement mode shapes can be obtained.

Due to the similarity of the strain modal formulation and the displacement modal formulation, the same modal identification methods can be used in both cases, as long as the appropriate caution is taken. In this article, the PolyMAX identification method [14] was used without any modifications.

11.3 FBG Measurement Principle

The fiber Bragg grating (FBG) is a periodic microstructure that acts as a wavelength selective mirror. This means that if light from a broadband source is injected in the optical fiber, only light within a very narrow spectral width, centered at the Bragg wavelength, will be back-reflected by the grating. The remaining light will continue its way through the optical fiber without experiencing any loss. The fiber Bragg grating is a symmetric structure, so it will always reflect light at the Bragg wavelength no matter which side the light is coming from.

The Bragg wavelength (λ_B) is essentially defined by the period of the microstructure (Λ) and the index of refraction of the core (n_{eff}):

$$\lambda_B = 2n_{\text{eff}}\Lambda \tag{11.9}$$

A fiber Bragg grating has unique characteristics to perform as a sensor. For example, when the fiber is stretched or compressed, the FBG will measure strain. This happens essentially because the deformation of the optical fiber leads to a change in the period of the microstructure and, consequently, of the Bragg wavelength. There is also some contribution from the variation of the index of refraction, through the photo-elastic effect. Sensitivity to temperature is also intrinsic to a fiber Bragg grating. In this case, the main contributor to Bragg wavelength change is the variation of the silica refraction index, induced by the thermo-optic effect. There is also a contribution from the thermal expansion, which alters the period of the microstructure. This effect is, however, marginal given the low coefficient of thermal expansion of silica.

The strain dependence of a fiber Bragg grating can be determined by differentiating the wavelength:

$$\frac{\Delta\lambda_B}{\lambda_B} = \frac{\Delta(n_{\text{eff}}\Lambda)}{n_{\text{eff}}\Lambda} = \left(1 + \frac{1}{n_{\text{eff}}} \cdot \frac{\partial n_{\text{eff}}}{\partial\varepsilon}\right)\Delta\varepsilon = (1 + p_e)\Delta\varepsilon = \beta_\varepsilon\Delta_\varepsilon \tag{11.10}$$

where β_ε is the strain sensitivity of the Bragg grating, p_e is the photo-elastic constant (variation of the index of refraction with axial tension), which for the optical fiber is equal to: $p_e \approx -0.212$, so the strain sensitivity of a FBG from (11.10) becomes:

$$\frac{\Delta\lambda_B}{\Delta_\varepsilon} = \beta_\varepsilon \cdot \lambda_B = 0.788\lambda_B \tag{11.11}$$

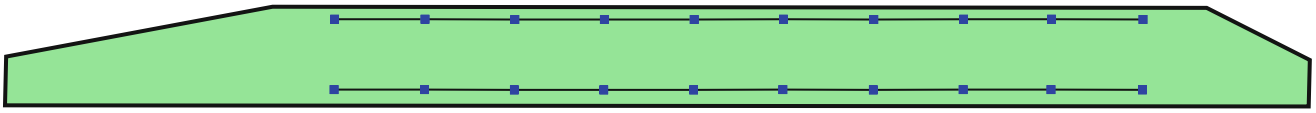

Fig. 11.1 Helicopter blade: location of FBG sensors and strain gauges

and therefore an FBG with wavelength $\lambda_B = 1,550\,\text{nm}$, will have the following sensitivity:

$$\frac{\Delta\lambda_B}{\Delta_\varepsilon} = 1.2\frac{pm}{\mu\varepsilon} \tag{11.12}$$

Multiple gratings can be used within a single fiber, as long as each one has a different wavelength. There are two methods of interrogating multiple wavelengths - a broadband light source that covers all the wavelengths, or a tunable light source that sweeps through all the wavelengths.

11.4 Experimental Analysis

Two analysis cases will be presented—initially, an experimental modal analysis on a helicopter main rotor blade will be shown. For this case, a standalone acquisition unit will be used, and the synchronization procedure with the rest of the electrical sensors will be described. Then a synchronized heterogeneous acquisition on the same structure will be carried out, with impact tests and the impulse responses from collocated strain gauges and FBG sensors will be shown.

11.4.1 Unsynchronized FBG Measurements

The main rotor blade of a PZL SW-3 helicopter was used for the strain modal analysis with the FBG sensors. For this experiment, the blade was suspended with elastic cords to obtain a free-free boundary condition and fiber bragg grating sensors were used to measure the dynamic strain on the surface of the blade. In total, 20 FBG sensors were instrumented on the surface of the blade, following two straight fiber lines of ten sensors each, and two strain gauges (in quarter bridge configuration) were used on one of the fiber lines to help with the synchronization. Figure 11.1 shows the position of the strain gauges and the FBG sensors on the two fiber lines on the surface of the blade.

The blade was excited using an electrodynamic shaker, and the driving point was chosen close to the tip of the blade, near the trailing edge, with a sine sweep excitation. Two acquisition units were used—an LMS Scadas Mobile with VB8 modules for the strain gauges and a separate acquisition unit for the FBG sensors—the interrogation method for this unit is based on a tunable light source that sweeps through all the FBG wavelengths. The excitation frequency ranged from 2 to 80 Hz, with the sampling rate from the FBG acquisition system being 200 Hz. In the specified bandwidth, 11 vibration modes were identified—six bending modes, three in-plane modes and two torsional modes. The natural frequencies and the mode types for these modes are shown on Table 11.1. The displacement modes of the blade (and their types) were already known from previous experiments [15].

The next step for the strain modal analysis using the FBG sensors is to synchronize their signals with the measured force signal. Since the resistive strain gauges, accelerometers and force cell signals were all acquired with the same acquisition unit and are therefore synchronized, the FBG sensors have only to be synchronize them with one of these sensors—hence, the use of the collocated strain gauges. This synchronization procedure is carried out in an offline manner, or practically speaking, after the data acquisition has already been done. The steps for the data synchronization are as follows:

- Selection of the best suitable strain gauge to be used for the synchronization
- Division of the data by blocks equal to number of averages
- Synchronization (alignment) of the data, block-by-block
- Reassembly of all the blocks in one data signal
- FRF calculation
- Data import into LMS Test.Lab for modal analysis

Table 11.1 Natural frequencies and mode types for the helicopter main rotor blade

Mode number	Natural frequency (Hz)	Damping ratio (%)	Mode type
1	3.6	1.72	Bending
2	10.3	0.50	Bending
3	14.0	0.84	In-plane
4	20.3	0.37	Bending
5	30.4	0.98	Torsional
6	33.8	0.4	Bending
7	37.6	0.66	In-plane
8	49.5	0.52	Bending
9	61.2	0.93	Torsional
10	67.2	0.43	Bending
11	75.9	0.74	In-plane

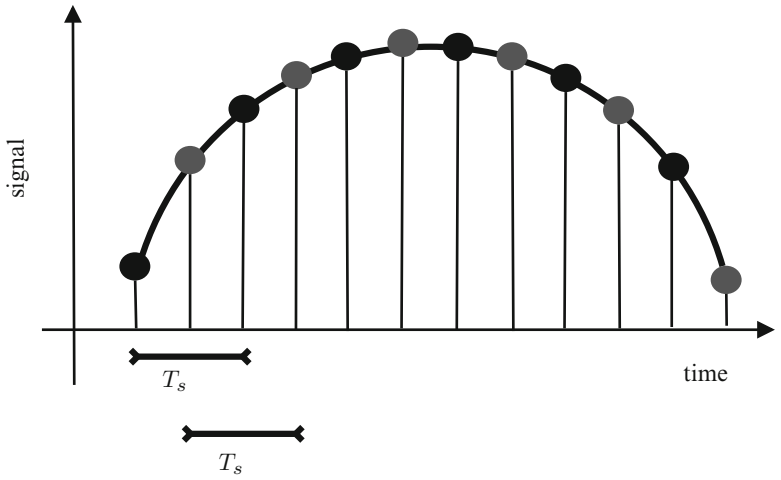

Fig. 11.2 Sampling time error example

After an initial analysis, the strain gauge and FBG sensor on point 4 (from Fig. 11.1) were chosen for the synchronization procedure—overall, all sensor pairs were suitable to be used, but one pair had to be chosen. Next, all signals were upsampled to improve the offline synchronization efficiency. This step can help to reduce errors—even if both signals would have the same sampling frequency, it is still possible that the samples are taken at a different time and therefore unsynchronized. Figure 11.2 shows an example of how this can happen—even though the sampling time T_s shown in the Figure is the same for both signals (black and grey), they can still be shifted in time. By reducing the sampling period T_s, one can reduce how big this error will be. The resampling factor for the strain gauge was of 4, and the resampling factor for the FBG sensor was of 16, bringing both sensors' sampling frequency up to 3,200 Hz.

Furthermore, the signals were divided by blocks—in total, they were divided in 20 blocks representing the 20 excitation cycles for the sine sweep. As a standard procedure, the first and last blocks are also discarded, so in the end 18 blocks were available. The next step is to align each block individually. This is carried out by using the cross-correlation function. For 2 very similar signals, synchronized in time, the cross correlation function should have its peak value exactly on the 0 lag position in the x-axis. If the signals are misaligned (which is our case), then the peak value will occur outside of the 0 lag position, but will represent how many lags (or sample differences) one of the signals should be shifted to be aligned. The result, after realigning all 18 blocks and putting them back together into one signal, is shown in Fig. 11.3, where one of the realigned blocks is shown.

Consequently, the FRFs can be computed by using the H1 estimator. To calculate the crosspower and autopower functions to be used in the H1 estimator calculations, a rectangular window was used and no overlap was performed (each block consisted of a full sweep, starting and ending with 0 excitation, so leakage was not a problem). The resulting FRFs for the one of the FBG and strain gauge sensor pairs and their respective coherence functions are shown in Fig. 11.4, where a comparison between the strain gauge and FBG signal quality can be made.

Finally, the FRFs can be imported in LMS Test.Lab so that the modal analysis can be carried out. For this purpose, only the FBG sensor FRFs are really needed, since the strain gauge measurements were only used initially for the synchronization. The procedure to identify the modes is the same as in the classic displacement modal analysis. The PolyMAX identification

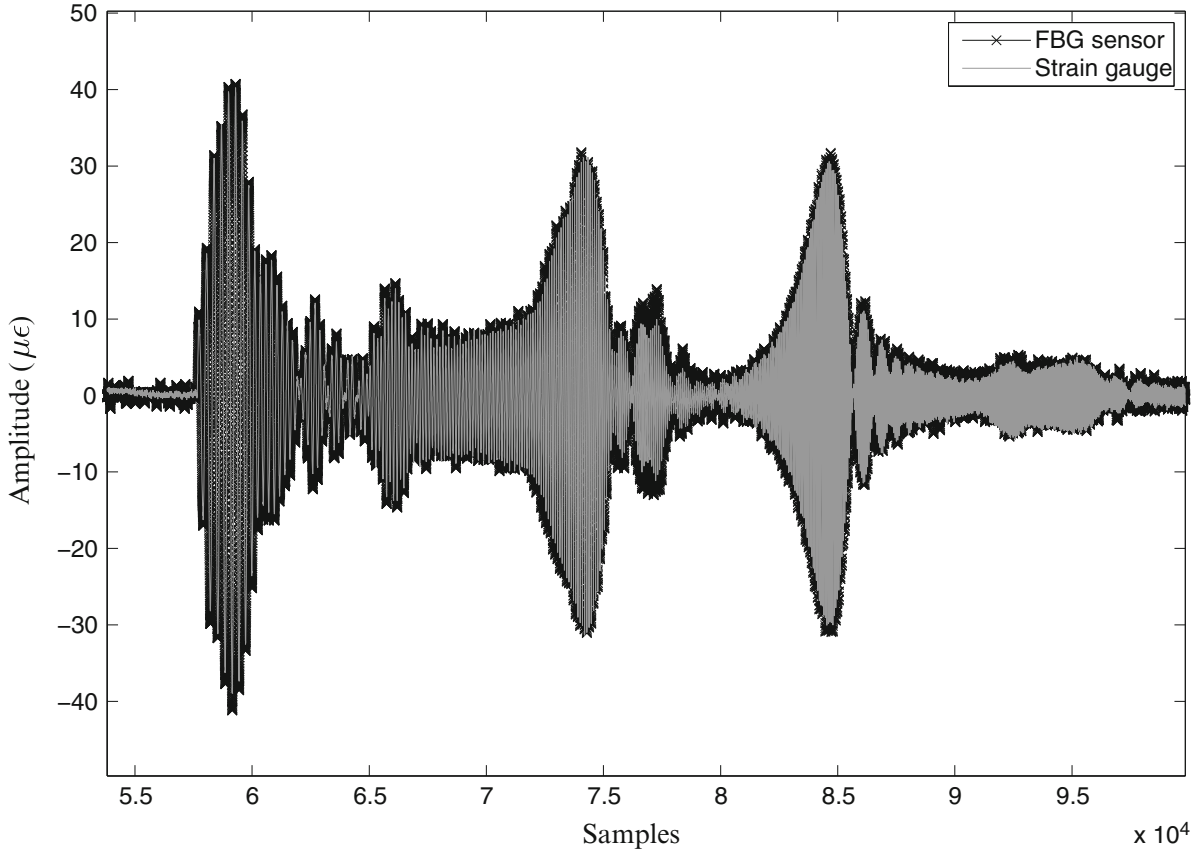

Fig. 11.3 FBG and strain gauge time signal alignment: zoomed in one of the blocks

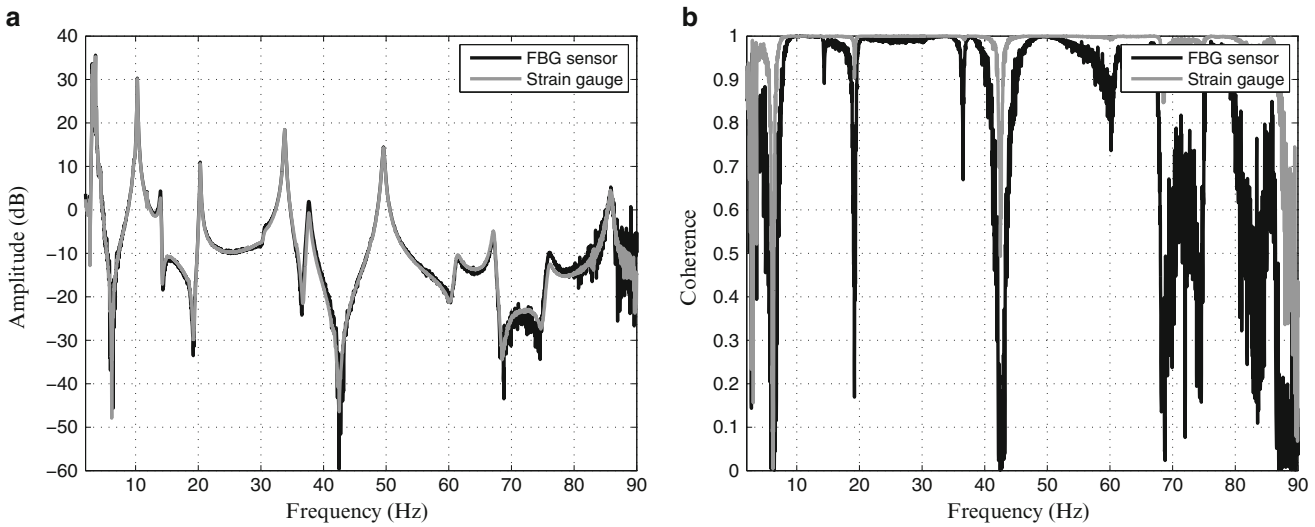

Fig. 11.4 Comparison of FRFs and coherence for one of the sensor pairs. (**a**) FRF comparison for sensor pair on point 4. (**b**) Coherence comparison for sensor pair on point 4

algorithm was used and all the 11 strain mode shapes shown in Table 11.1 were identified. The first five of these mode shapes are shown in Figs. 11.5, 11.6, 11.7, 11.8, and 11.9.

Analyzing the acquired data from the strain gauges and FBG sensors, it is visible that the FRFs match very well up to 65 Hz. After this frequency, there is more noise present on the FBG FRF (Fig. 11.4a), which is also visible in the coherence function Fig. 11.4b. This decrease in quality can be attributed to two facts—as the frequency gets closer to the maximum

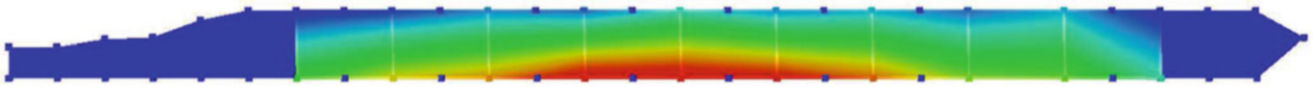

Fig. 11.5 Helicopter blade strain mode—first bending mode at 3.58 Hz

Fig. 11.6 Helicopter blade strain mode—second bending mode at 10.27 Hz

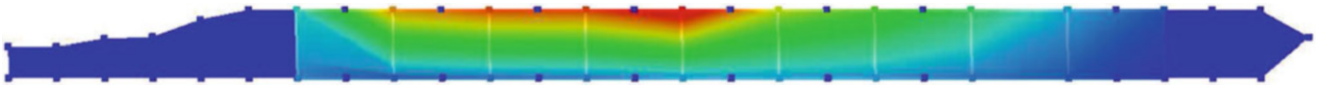

Fig. 11.7 Helicopter blade strain mode—first in-plane mode at 13.9 Hz

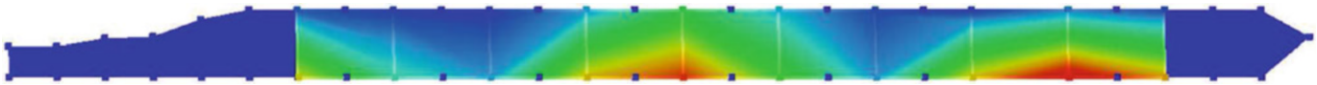

Fig. 11.8 Helicopter blade strain mode—third bending mode at 20.30 Hz

sensor bandwidth (100 Hz), it is expected that the quality might decrease. Moreover and most importantly, the described offline synchronization procedure works better for lower frequencies, while in higher frequencies it is still expected that the synchronization will not be perfect, which is the case for the FBG sensors.

11.4.2 Synchronized Measurements

The way that the measurements were carried out with the FBG sensors meant that the quality was limited by the offline synchronization procedure. To overcome this problem, a different methodology for interrogating the FBG wavelengths was used by using a broadband light source that covers all the FBG wavelengths. In this way, it is possible to obtain an analogue signal from the FBG sensors, which can be connected directly to the same acquisition system as the other sensors, guaranteeing synchronous measurements with higher sampling rates. The downside is that less sensors are supported per fiber, as the broadband light source has a much more limited bandwidth.

To check for synchronicity between the sensors, impact tests were carried out, measuring the signals from two FBG sensors and collocated resistive strain gauges, their position number (4 and 7) shown in Fig. 11.1 an both sensor pairs can be seen in Fig. 11.10.

The time trace for the impulse response of the sensor pairs can be seen in Fig. 11.11a and b. In this case, no synchronization procedure was necessary, as the sensor acquisition is done using the same acquisition unit. Furthermore, the noise levels for both sensor types was investigated. Figure 11.12 shows the noise levels for both types of sensors. The FBG sensor has lower noise level and additionally, there is a high amplitude harmonic component at 50 Hz on the quarter bridge strain gauge, due to the noise from the electrical network.

11.5 Results Analysis and Conclusion

In this paper, the theory for strain modal analysis was presented, followed by an introduction on the measurement principle for Fiber Bragg Grating sensors. For this purpose, a brief explanation of the basic properties of the sensor were given and how it can be used to measure strain.

Moreover, it was shown how FBG sensors can be used to carry out a strain modal analysis and visualize the strain mode shapes. To be able to properly do the modal identification procedure, an offline synchronization procedure had to be carried out, as a means of synchronizing the signals from the FBG sensors to the signal from the force sensor. The results show that

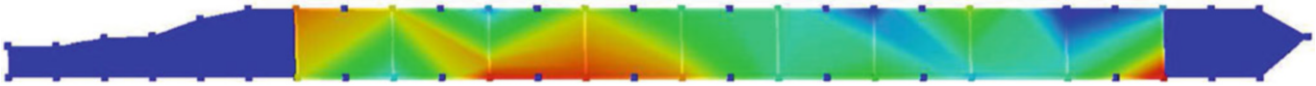

Fig. 11.9 Helicopter blade strain mode—first torsional mode at 30.4 Hz

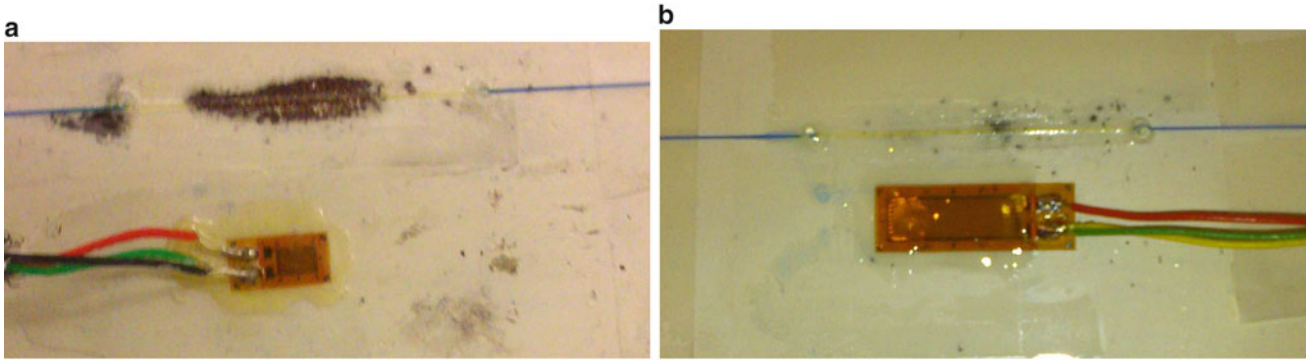

Fig. 11.10 Collocated FBG sensors and strain gauges on helicopter blade. (**a**) FBG sensor and strain gauge collocated on point 4. (**b**) FBG sensor and strain gauge collocated on point 7

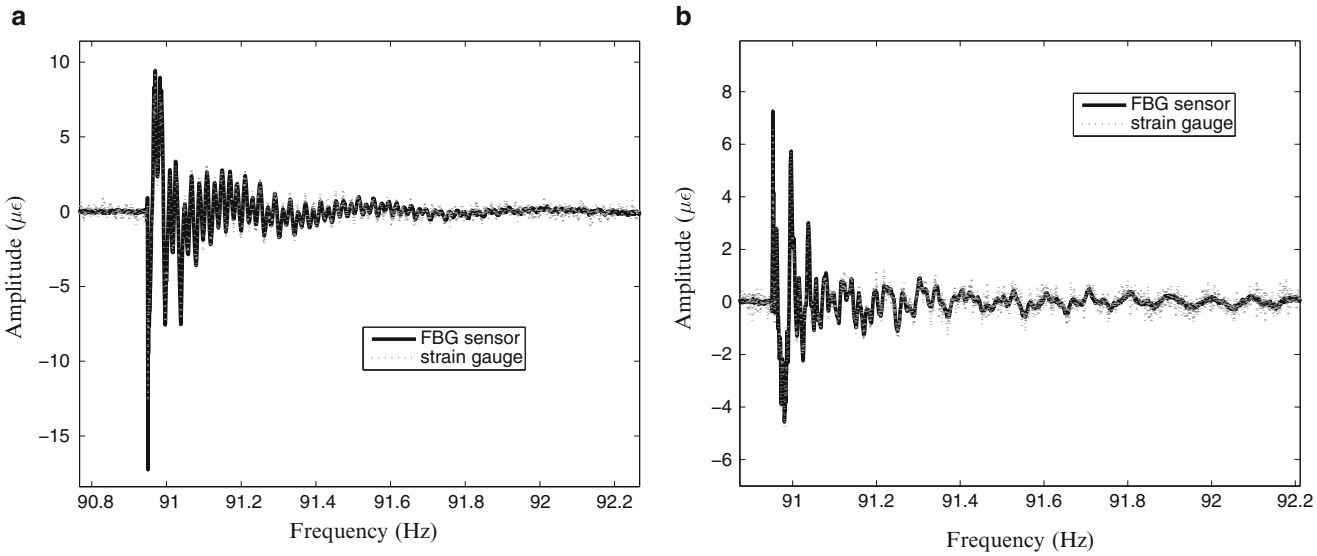

Fig. 11.11 Impulse response for sensor pairs on locations 4 and 7 on blade. (**a**) FBG and strain gauge impulse response: synchronized signal acquisition on point 4. (**b**) FBG and strain gauge impulse response: synchronized signal acquisition on point 7

the strain mode shapes can be identified, but there is a limitation on the fact that the offline synchronization procedure is less efficient as the frequency gets higher. To overcome this limitation, a different acquisition principle for the FBG sensors was used, which could yield as an output an analogue signal that could be directly acquired by the same acquisition unit as the electrical sensors, guaranteeing synchronization. A noise analysis of both strain gauges and FBG sensors was carried out, and it was seen that the FBG could yield lower levels of noise.

Future studies include more complex measurements and a full modal analysis with the synchronized FBG sensors and use of the sensors in other strain applications.

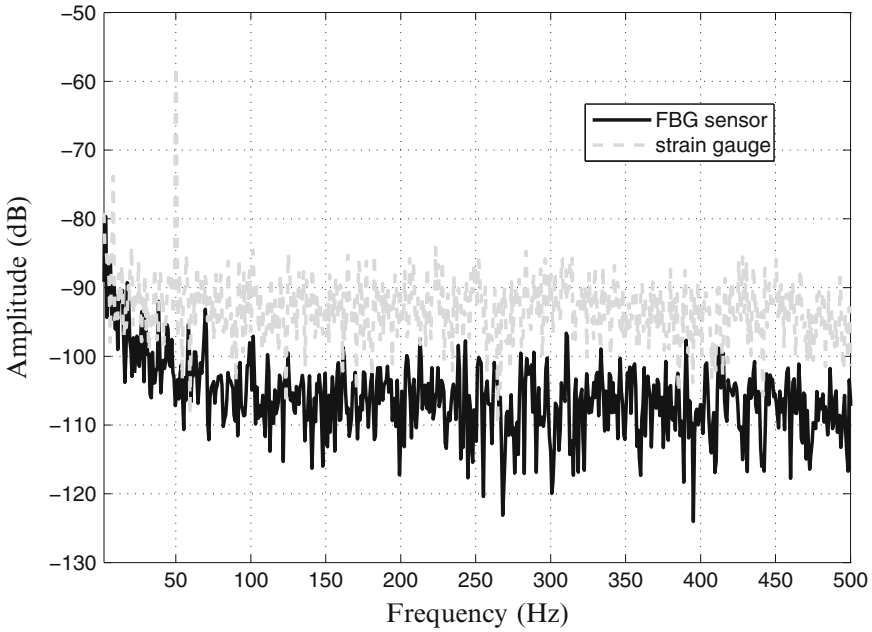

Fig. 11.12 FBG sensor and strain gauge noise levels

Acknowledgements Fábio Luis Marques dos Santos, first author of this paper, is an Early Stage Researcher at Siemens Simulation & Test Solutions, under the FP7 Marie Curie ITN project "IMESCON" (FP7-PEOPLE-2010-ITN, Grant Agreement No. 264672). This research was also carried out in the Framework of FP7 ICT Collaborative project "WiBRATE" (FP7-ICT-2011-7, Grant Agreement No. 289041). The authors of this work gratefully acknowledge the European Commission for the support.

References

1. Vandepitte D, Sas, P (1990) Case study of fracture of a mechanical component due to resonance fatigue. Mech Syst Sig Process 4(2):131–143.
2. Liefooghe C, Van der Auweraer H, Janssen P, Sas P (1992) Validation of modal filtering/editing approach to dynamic fatigue analysis. In: Proceedings of ISMA 17, Tokyo
3. Wentzel H (2013) Fatigue test load identification using weighted modal filtering based on stress. Mech Syst Sig Process 40:618–627
4. Bernasconi O, Ewins DJ (1989) Application of strain modal testing to real structures. In: Proceedings of the 7th international modal analysis conference, vol 2, pp 1453–1464
5. Vári LM, Heyns PS (1994) Using strain modal testing. In: Proceedings of the 12th international conference on modal analysis, vol. 2251, p 1264
6. Li S, Wu Z (2005) Structural identification using static macro-strain measurements from long-gage fiber optic sensors. J Appl Mech 8:943–948
7. Reich GW, Park KC (2001) A theory for strain-based structural system identification. J Appl Mech 68(4):521–527
8. Peeters B, Luis Marques dos Santos F, Pereira A, Araujo F (2014) On the use of optical fiber bragg grating (fbg) sensor technology for strain modal analysis. In: 11th international conference on vibration measurements by laser and noncontact techniques-AIVELA 2014: Advances and applications, vol 1600. AIP Publishing, New York, pp 39–49
9. Kranjc T, Slavič J, Boltežar M (2014) A comparison of strain and classic experimental modal analysis. J Vib Control. doi: 1077546314533137
10. Kang L-H, Kim D-K, Han J-H (2007) Estimation of dynamic structural displacements using fiber bragg grating strain sensors. J Sound Vib 305(3):534–542
11. Ling H-Y, Lau K-T, Cheng L (2004) Determination of dynamic strain profile and delamination detection of composite structures using embedded multiplexed fibre-optic sensors. Compos Struct 66(1):317–326
12. Pisoni AC, Santolini C, Hauf DE, Dubowsky S (1995) Displacements in a vibrating body by strain gage measurements. In: Proceedings of the 13th international conference on modal analysis
13. Tourjansky N, Edmond S (1992) The measurement of blade deflections - a new implementation of the strain pattern analysis. ONERA Technical Paper
14. Peeters B, Van der Auweraer H, Guillaume P, Leuridan J (2004) The polymax frequency-domain method: a new standard for modal parameter estimation? Shock Vib 11:395–409
15. Luis Marques dos Santos F, Peeters B, Van der Auweraer H, Carlos Sandoval Góes L (2013) Modal-based damage detection of a composite helicopter main rotor blade. 54th AIAA/ASME/ASCE/AHS/ASC structures, structural dynamics, and materials conference